Eletrônica de Potência
Open Journal of Power Electronics

Received June 11, 2024; accepted December 23, 2024; Date of publication January 21, 2025.
The review of this paper was arranged by Associate Editor Mokhtar A. Ahmed and Editor-in-Chief Heverton A. Pereira.

Digital Object Identifier http://doi.org/10.18618/REP.e202509

Dual Input Interleaved Three-Phase Rectifier In Discontinuous Conduction Mode For Application In Small Wind Turbines

Guilherme M. Todys[1,*], Luís P. Custódio[1], Alceu A. Badin[2], Amauri A. Assef[2], Roger Gules[2], Delvanei G. Bandeira Jr.[1], Eduardo F. R. Romaneli[1], Daniel F. Cortez[1]

[1]Universidade Tecnológica Federal do Paraná (UTFPR), PPGSE – Curitiba, PR, Brasil.
[2]Universidade Tecnológica Federal do Paraná (UTFPR), CPGEI – Curitiba, PR, Brasil.

e-mail: guilhermemtodys@gmail.com*; luiscustodio@alunos.utfpr.edu.br; badin@utfpr.edu.br; amauriassef@utfpr.edu.br; rgules@gmail.com; delvaneijunior@utfpr.edu.br; felix@utfpr.edu.br; danielcortez@utfpr.edu.br
*Corresponding author

ABSTRACT This paper presents a high-gain three-phase interleaved rectifier operating in DCM, with dual input, for application in small wind generators. The two input diode bridges promote the sharing of the current, resulting in a significant reduction of the converter's current stresses when compared to previous topologies. A theoretical analysis of the proposed converter was performed, followed by a simulation study, and experimental tests with a physical prototype. The simulations compared the proposed three-phase rectifier with three other three-phase topologies, demonstrating its operation with significantly reduced current stresses and smaller input inductors. The experiments compared the operation of the converter when working with a three-phase power supply, and a wind turbine in association with an MPPT method using the Perturb and Observe (P&O) technique. For an output power of 1 kW, on a 400 V DC bus and an input RMS line voltage of 114 V, the structure's obtained efficiency was higher than 95%. Furthermore, the experimental results confirmed that the rectifier operates with sinusoidal input currents, low current ripple, and high power factor for all the tested scenarios.

KEYWORDS Three-phase rectifier, Discontinuous Conduction Mode, Three-phase interleaved rectifier

I. INTRODUCTION

Due to the growing demand for energy worldwide, combined with the need to reduce environmental impacts related to its production, renewable energy sources are considered essential for diversifying and expanding a country's energy matrix [1]–[5]. In this scenario, wind energy has been widely studied, gaining particular notoriety in recent years, presenting a generation capacity with a tendency of growth at a global level [1]–[3], [6], [7].

In wind systems, the conversion of wind energy into electrical energy is done by using a wind turbine and an electrical generator [8]. Small wind generators, with a power range between 1 kW and 15 kW, are used in situations where the implementation of larger generators is unfeasible, as is the case in urban areas [9]–[11]. In small systems, the wind turbine is used with a permanent magnet synchronous generator (PMSG), operating with a variable output frequency and low voltage, due to the wind speed variation. Therefore, for the system to be connected to the grid, it is necessary to use static converters to adapt the generated energy to the desired standards, with two types of converters being used to carry out this task: a rectifier followed by an inverter [9], [10].

Regarding the rectifier stage, the most basic topology mentioned in the literature is the diode bridge rectifier [11], [12]. Although this topology is simple, with few components and low implementation cost, it has a low input power factor, due to the current with high total harmonic distortion (THD) drained from the PMSG. Moreover, it is unfeasible to track the maximum power point (MPP) in this type of rectifier, making this topology unsuitable for wind generation [11], [12]. A more appropriate option for application in small wind conversion systems is the three-phase boost rectifier operating in discontinuous conduction mode (DCM) [13], [14]. This topology presents a significant improvement regarding the power factor, as well as the THD of the input current, compared to the diode bridge rectifier in its most basic configuration. However, its operation presents high current stress and low-frequency distortion in the input current, in addition to requiring the use of a high-frequency filter at the converter input. An improvement of such topology can be found in the three-phase boost DCM multiphase rectifier [15], where current stress is reduced as a consequence of multiphase operation and the need for the input filter is eliminated. Nevertheless, the low-frequency interference in the input current remains present. Furthermore, the rectifier

CC BY

introduced in [16], presents even lower current stress in the switches, in addition to reducing the low-frequency interference in the input current. Based on such topology, the three-phase three-level DCM interleaved boost rectifier, proposed in [17], was developed, presenting improvements, such as reducing the voltage stress on the switches to half of the output voltage, in addition to a greater static gain, while maintaining the positive aspects of [16].

The topology presented in this article is based on the three-level DCM interleaved boost rectifier [17], and aims to further improve the matter concerning the structure's current stresses, promoting a considerable reduction through an operation with a double input rectifier bridge. The proposed topology is presented in Section II of this paper, which includes a description of its principle of operation, a theoretical analysis of the converter, and a description of the maximum power point tracking (MPPT) method used in the experiments. In Section III, a simulation study was conducted, presenting a comparative evaluation of the proposed rectifier against three other three-phase rectifier topologies. Section IV presents the experimental results, and the conclusions are provided in Section V. Lastly, Section VI is dedicated to acknowledgments.

II. PROPOSED THREE-PHASE RECTIFIER

The topology of the proposed three-phase rectifier is presented in Fig. 1. In this double-input circuit, despite having six inductive elements at the input, the current stresses are divided between the switching legs through the two three-phase bridges, thus reducing the current stress on both the inductors and the switches. It is worth mentioning that switches S_1, S_4, S_5, and S_8 could be replaced with diodes without affecting the converter's operation. However, in order to prioritize the reduction of the structure's conduction losses, the switches were maintained.

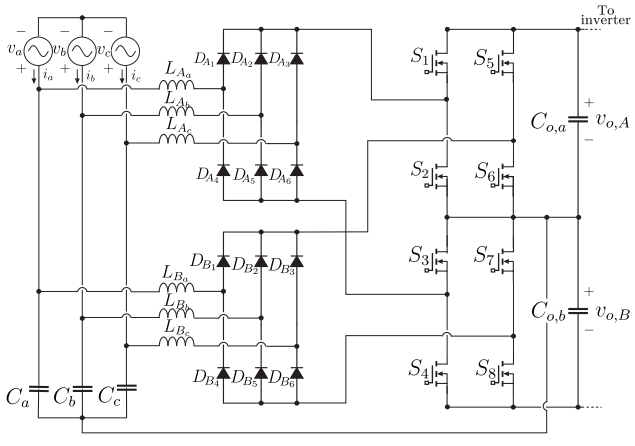

FIGURE 1. Dual Input Interleaved DCM Three-Phase Rectifier.

A. Principle of Operation

To detail the topological stages of the converter operating in discontinuous conduction mode, an interval of $60°$ (from $120°$ to $180°$) of the electrical operation cycle ($0°$ to $360°$) was considered. For switching commands, the duty cycle (D) is considered fixed, with D = 0.5, and switches S_2-S_4/S_5-S_7 operate with a phase difference of $180°$ in relation to switches S_1-S_3/S_6-S_8.

In the first operation stage, as depicted in Fig. 2(a), switches S_2-S_4/S_5-S_7 are commanded to conduct, and diodes D_{A_1}, D_{A_2}, D_{A_6}, D_{B_1}, D_{B_2} and D_{B_6} are conducting. In this condition, energy is stored in inductors L_{A_a}, L_{A_b} and L_{B_c} through switches S_2 and S_7, while energy is transferred from inductors L_{A_c}, L_{B_a} and L_{B_b} through switches S_4 and S_5.

In operation steps 2, 3, and 4, respectively shown in Fig. 2(b), Fig. 2(c), and Fig. 2(d), the energy transfer process of inductors L_{B_b}, L_{B_a} and L_{A_c} is completed. Also, diodes D_{B_2}, D_{B_1} and D_{A_6} are reversed biased, respectively.

In operation step 5, as illustrated in Fig. 2(e), switches S_1-S_3/S_6-S_8 are commanded to conduct, and diodes D_{A_1}, D_{A_2}, D_{A_6}, D_{B_1}, D_{B_2} and D_{B_6} are conducting. In this condition, energy is stored in inductors L_{A_c}, L_{B_a} and L_{B_b} through switches S_3 and S_6, while energy is transferred from inductors L_{A_a}, L_{A_b} and L_{B_c} through switches S_1 and S_8.

In operation steps 6, 7, and 8, respectively shown in Fig. 2(f), Fig. 2(g) and Fig. 2(h), the energy transfer process of inductors L_{A_b}, L_{A_a} and L_{B_c} is completed. Also, diodes D_{A_2}, D_{A_1} and D_{B_6} are reverse biased, respectively.

The waveforms corresponding to the described operation steps are shown in Fig. 3. The current signals of switches S_5, S_6, S_7 and S_8 are equivalent to the ones of switches S_1, S_2, S_3 and S_4 with a phase shift of $180°$.

B. Theoretical analysis

The mathematical analysis of the presented rectifier is based on [18], [19] and [20].

The value of the input inductance is obtained through (1):

$$L_{in} = \frac{3\sqrt{3}DV_p^2}{4P_{in}f_s}. \tag{1}$$

Where,

- V_p is the peak value of the input phase voltage [V];
- D is the converter's duty cycle;
- P_{in} is the input power [W];
- f_s is the switching frequency [Hz].

The peak value of the current flowing through the input inductors ($I_{p_{L_{in}}}$) is determined by (2):

$$I_{p_{L_{in}}} = \frac{2\sqrt{3}V_pD}{3L_{in}f_s}. \tag{2}$$

The ratio between the peak value of the input voltage (V_p) and the output voltage (V_o) is given by α, obtained through (3):

$$\alpha = \frac{V_p}{V_o}. \tag{3}$$

The expression to calculate the RMS value of the input current ($I_{ine f}$) is shown in (4):

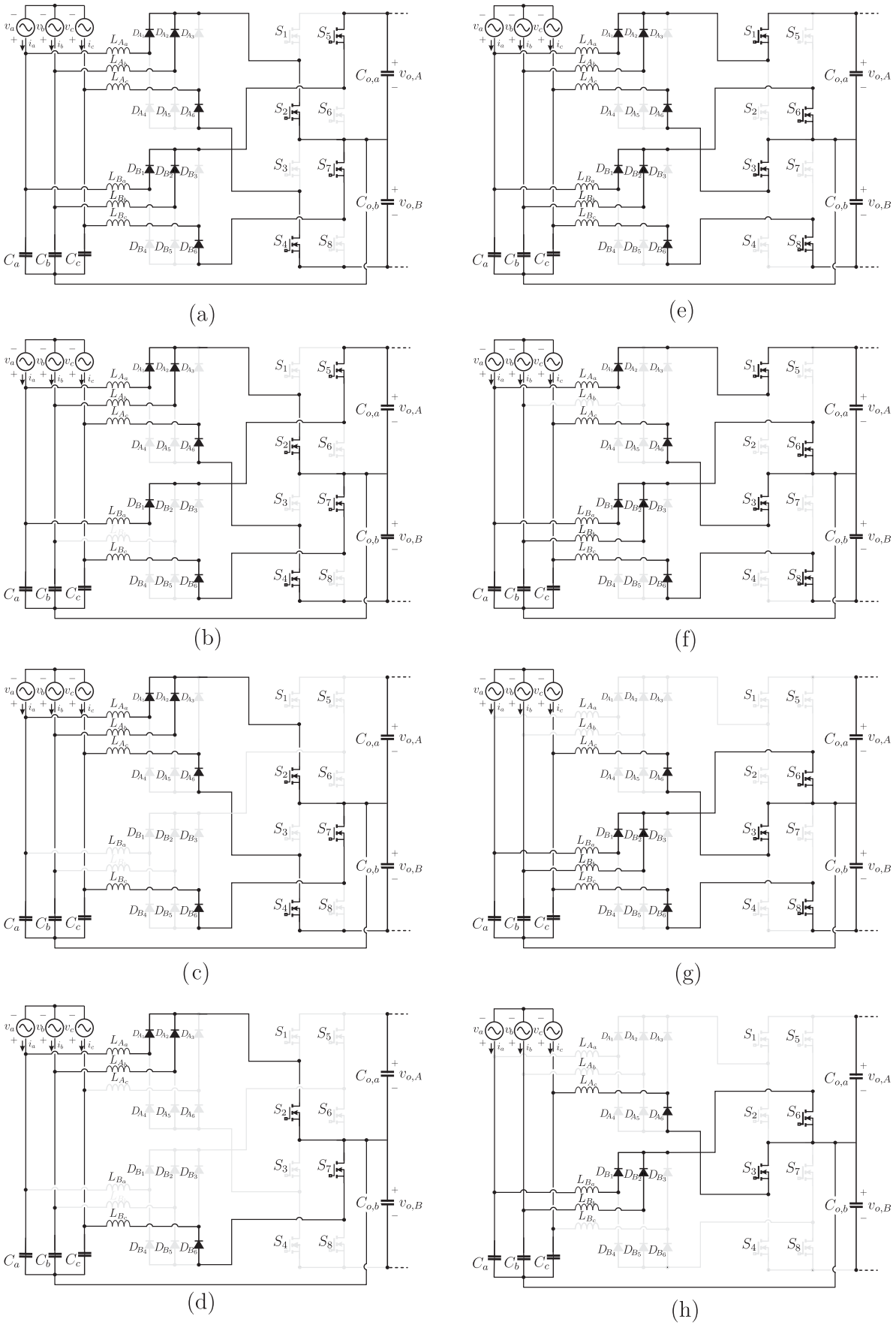

FIGURE 2. Rectifier operation stages.

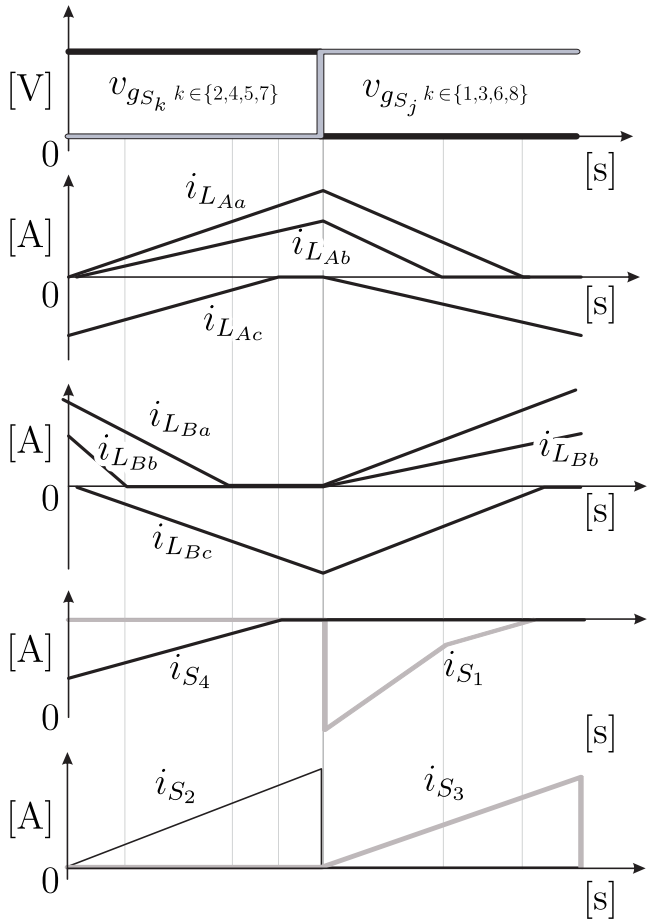

FIGURE 3. Theoretical rectifier's waveforms.

$$I_{inef} = \frac{V_o D^2 \sqrt{\alpha}}{f_s L_{in} \sqrt{\pi}}. \tag{4}$$

The power factor (PF) and THD can be obtained using (5) and (6), respectively:

$$PF = \frac{\frac{\sqrt{2}}{\sqrt{\alpha}+\sqrt{\pi}} \left[-2 - \frac{\pi}{\alpha} + \frac{2}{\alpha\sqrt{1-\alpha^2}}\beta \right]}{\sqrt{\frac{2}{1-\alpha^2} + \frac{\pi}{\alpha} + \frac{2\alpha^2-1}{\alpha(1-\alpha)^2} + \frac{2}{\sqrt{1-\alpha^2}}\beta}}, \tag{5}$$

$$THD = \sqrt{\frac{1}{PF^2} - 1}. \tag{6}$$

Where, β is obtained through (7):

$$\beta = \frac{\pi}{2} + \arctan\left(\frac{\alpha}{\sqrt{1-\alpha^2}}\right). \tag{7}$$

Regarding the current stress in the switches, (8) and (9) present the expressions for calculating the average and RMS current values in the switches S_1, S_4, S_5 and S_8:

$$I_{S_k,med} = \frac{3V_p D^2}{L_{in} f_s \pi}, \tag{8}$$

$$I_{S_k,rms} = \frac{\sqrt{3}V_p}{L_{in} f_s} \sqrt{\frac{D^3}{\pi}}, \tag{9}$$

where $k \in \{1, 4, 5, 8\}$.

Considering switches S_2, S_3, S_6 and S_7, the average and RMS values of the current flowing through these components can be obtained by utilizing (10) and (11):

$$I_{S_n,med} = \frac{2V_p D^2}{L_{in} f_s \pi}, \tag{10}$$

$$I_{S_n,rms} = \frac{\sqrt{2}V_p \sqrt{D^3}}{2L_{in} f_s}, \tag{11}$$

where $n \in \{2, 3, 6, 7\}$.

The voltage to which the diodes and switches are subjected has the same peak value, expressed by (12):

$$V_{D_p} = V_{S_p} = -\frac{V_o}{2}. \tag{12}$$

The input capacitance value for the three phases $(C_k, k \in a, b, c)$ is calculated considering the load variation (ΔQ) and the input capacitor voltage ripple $(\Delta V_{C_{in}})$. Equation (13) presents the resulting expression:

$$C_{in} = \frac{\Delta Q}{\Delta V_{C_{in}}} = \frac{I_{p_{L_{in}}}}{8 f_s \Delta V_{C_{in}}}. \tag{13}$$

The output capacitance (C_o) has its value estimated by the output power, P_o, and by the variation in the output voltage, ΔV_{C_o}, as shown in (14):

$$C_o = \frac{P_o}{2\pi f_s V_o \Delta V_{C_o}}. \tag{14}$$

C. MPPT method

When powered by the wind turbine, the MPPT strategy applied to the rectifier utilizes the Perturb and Observe (P&O) method, with the duty cycle (*D*) as the chosen control variable [21], [22].

The method implementation relies on the calculation of the input power based on measurements of the three-phase voltages and currents. It compares the calculated power of a given iteration k with the value calculated in the previous iteration $(k-1)$ to determine whether the power increased or decreased. Likewise, it evaluates the variation of the control variable, *D*, between the previous and current iterations. Finally, based on the results of the preceding steps, the duty cycle is updated accordingly. The schematic of control of the described MPPT method is detailed in Fig. 4, and Fig. 5 illustrates the algorithm's logic.

III. SIMULATION ANALYSIS: COMPARATIVE EVALUATION WITH OTHER THREE-PHASE RECTIFIER TOPOLOGIES

In order to promote a more in-depth analysis of the differences and advantages of the three-phase rectifier proposed in this paper, a simulation study was performed utilizing the software PSIM, version 2022.3. The aim of this study is to compare the proposed three-phase rectifier with three other three-phase topologies suitable for small

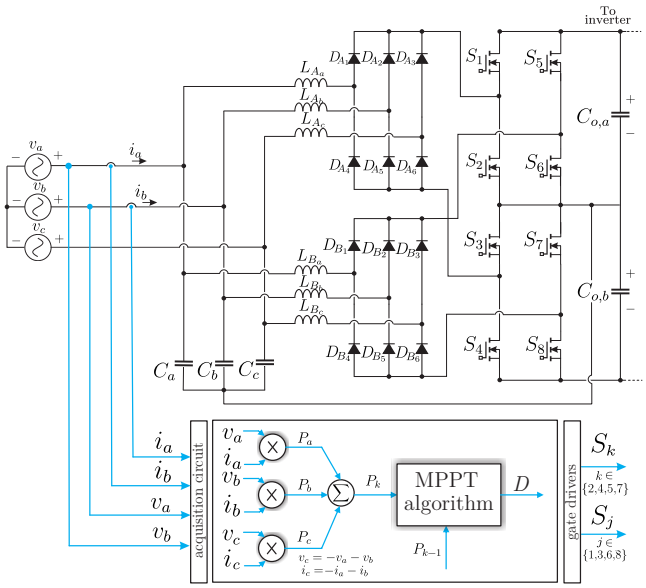

FIGURE 4. MPPT control schematic.

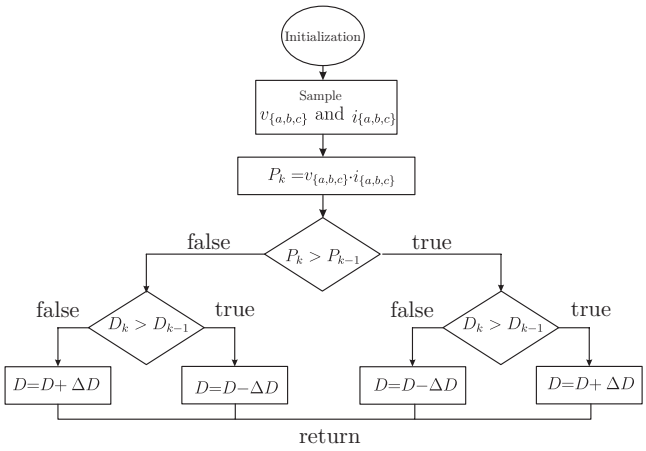

FIGURE 5. MPPT algorithm block diagram.

wind turbine generation. The selected rectifiers include the two-level three-phase boost CCM rectifier [23], the three-phase boost DCM rectifier [13], [14], and the three-level three-phase interleaved boost DCM rectifier [17]. The same project specifications were considered for all rectifiers. Table I presents a comparison between the rectifiers in terms of the number of components, while Table II provides information on the operating parameters of each rectifier.

Since the rectifier presented in this paper can still operate properly when switches S_1, S_4, S_5, and S_8 are replaced with diodes, two possible configurations will be considered for the component quantity comparison, presented in Table I: configuration 01 (Config 01) includes switches S_1, S_4, S_5, and S_8, while configuration 02 (Config 02) replaces these switches with diodes. As a result, the two configurations will differ in the number of diodes and switches used. As shown in the results of Table II, the current stresses throughout the entire structure of the proposed three-phase rectifier, including the inductors, switches, and output capacitors, were significantly reduced compared to the other two topologies operating in DCM. Furthermore, these values are close to those obtained for the CCM topology but with input inductances approximately 15 times smaller. Therefore, although the proposed converter presents six input inductors, as shown in Table I, the reduced current stress and lower inductance values decrease both the cost and volume of these components compared to the DCM and CCM structures, which utilize only three input inductors.

Furthermore, the waveform of input current of phase A (i_a), for each rectifier topology considered in the simulation analysis, is shown in Fig. 6(a), Fig. 6(b), Fig. 6(c) and Fig. 6(d), respectively. For the three-level three-phase interleaved boost DCM rectifier [17] and the dual input interleaved DCM three-phase rectifier, an input series inductance of 300 μH was considered in order to emulate the presence of a wind turbine at the system's input. The input PF and the THD of the input current i_a are presented in Table III. From the analysis of Fig. 6 and Table III, it can be concluded that all tested topologies achieved a high power factor and low THD. Additionally, in a real-world application, where the rectifier is connected to a wind turbine, the turbine's inductance would further reduce the THD across all rectifiers.

To evaluate the switching losses in the rectifiers, Fig. 7 presents the voltage and current waveforms, v_s and i_s, for one switch in each rectifier topology. In order to improve the visualization of the current's waveforms, the current was multiplied by a factor of 20, so current and voltage signals could be more easily analyzed and compared. As illustrated in Fig. 7(a) the CCM topology exhibits dissipative switching, with the switch voltage stress equal to the DC bus voltage (400 V). In contrast, since the other three topologies operate in DCM, Fig. 7(b), Fig. 7(c) and Fig. 7(d) show Zero Current Switching (ZCS), with zero current through the switch at turn-on. Additionally, in both the three-level three-phase interleaved Boost DCM Rectifier [17] and the dual input interleaved DCM three-phase rectifier—both three-level topologies—the voltage stress on switches is reduced to half that of the CCM topology and the other DCM topology, equaling half the DC bus voltage (200 V). Consequently, switching losses are significantly higher in the CCM topology due to the combination of dissipative switching, elevated voltage stress on switches, and diode reverse recovery, which further increases switching losses.

Considering the use of conventional silicon (Si) switches, the IGBT is the suitable power switch for the two-level CCM rectifier due to the highest voltage stress (400 V) and the presence of ultra-fast intrinsic switch diode. The CCM operation results in a high reverse recovery current, increasing the switch turn-on losses. Thus, the use of MOSFET is not recommended for this topology due to the slow intrinsic diode that significantly increases the switch turn-on losses and the high conduction losses for high voltage level operation. However, the IGBT presents the tail current increasing

CC BY

TABLE I. Component Quantity Comparison Across the Four Three-Phase Rectifier Topologies

Topology	Inductors	Capacitors	Switches	Diodes
Two-level three-phase boost CCM rectifier [23]	3	1	6	0
Three-phase boost DCM rectifier [13], [14]	3 + 3(filter)	1 + 3(filter)	1	7
Three-level three-phase interleaved boost DCM rectifier [17]	3	5	2	8
Dual input interleaved three-phase rectifier	6	5	Config 01: 8 Config 02: 4	Config 01: 12 Config 02: 16

TABLE II. Operation Parameters Comparison Across the Four Three-Phase Rectifier Topologies

Operation parameters	**Two-level three-phase boost CCM rectifier** [23]	**Three-phase boost DCM rectifier** [13], [14]	**Three-level three-phase interleaved boost DCM rectifier** [17]	**Dual input interleaved three-phase rectifier**
Does it require a three-phase LC input filter?	No	Yes	No	No
Input RMS Line Voltage	114 V	114 V	114 V	114 V
Switching Frequency	20 kHz	50 kHz	51.4 kHz	51.4 kHz
Output Power	1 kW	1 kW	1 kW	1 kW
Output Voltage	400 V	400 V	400 V	400 V
Input Capacitor Value	-	-	5.29 μF	1.6 μF
Input Capacitor - Peak Current	-	-	5.99 A	1.05 A
Input Capacitor - RMS Current	-	-	3.28 A	0.36 A
Input Inductor Value	1.662 mH	46 μH	65.3 μH	109.48 μH
Input Inductor - Peak Current	7.14 A	20.15 A	15.4 A	7.54 A
Input Inductor - RMS Current	5.05 A	9.46 A	6.94 A	3.07 A
Output Capacitor Value	235 μF	235 μF	2x470 μF	2x470 μF
Output Capacitor - Peak Current	5.18 A	17.58 A	13.34 A	7.24 A
Output Capacitor - RMS Current	3.21 A	6.06 A	4.46 A	2.56 A
Switches - Peak Current	7.9 A	17.59 A	20.08 A	9.69 A
Switches - RMS Current	3.61 A	8.6 A	8.23 A	3.31 A
Switches - Voltage Stress	400 V	400 V	200 V	200 V

TABLE III. Simulation Analysis - Power Factor and THD of the Studied Rectifiers

Topology	PF	THD (%)
Two-level three-phase boost CCM rectifier [23]	0.999	4.08
Three-phase boost DCM rectifier [13], [14]	0.997	5.21
Three-level three-phase interleaved boost DCM rectifier [17]	0.999	2.36
Dual input interleaved three-phase rectifier	0.995	2.86

the turn-off losses, limiting the switching frequency lower than 30 kHz.

The MOSFET switch is recommended for the DCM topologies due to the ZCS turn-on without the reverse recovery of the intrinsic diodes. For this reason, the slow intrinsic diode of the MOSFET is not a problem for the DCM operation. The lowest voltage stress of the three-level topologies (200 V) allows the use of very low conduction losses MOSFET with reduced turn-off switching losses compared to the two-level CCM rectifier. As a result, the DCM rectifiers are usually designed with switching frequency higher than the CCM rectifiers.

Therefore, to ensure a fair comparison, the switching frequency for the two-level three-phase boost CCM rectifier was set to 20 kHz in the simulation analysis. In contrast, the DCM topologies operated at higher switching frequencies, being 50 kHz or above.

Additionally, the design of the input inductors for each rectifier was carried out, and the results are presented in Table IV. The 'Total volume' column presents the combined volume of all inductors used in the respective converter topology. The analysis of the data in Table IV confirms that, as expected, the core designed for the proposed rectifier has the smallest volume. It is nearly five times smaller than the core used in the CCM topology and about twice as small as the cores in the other DCM topologies. This is due to

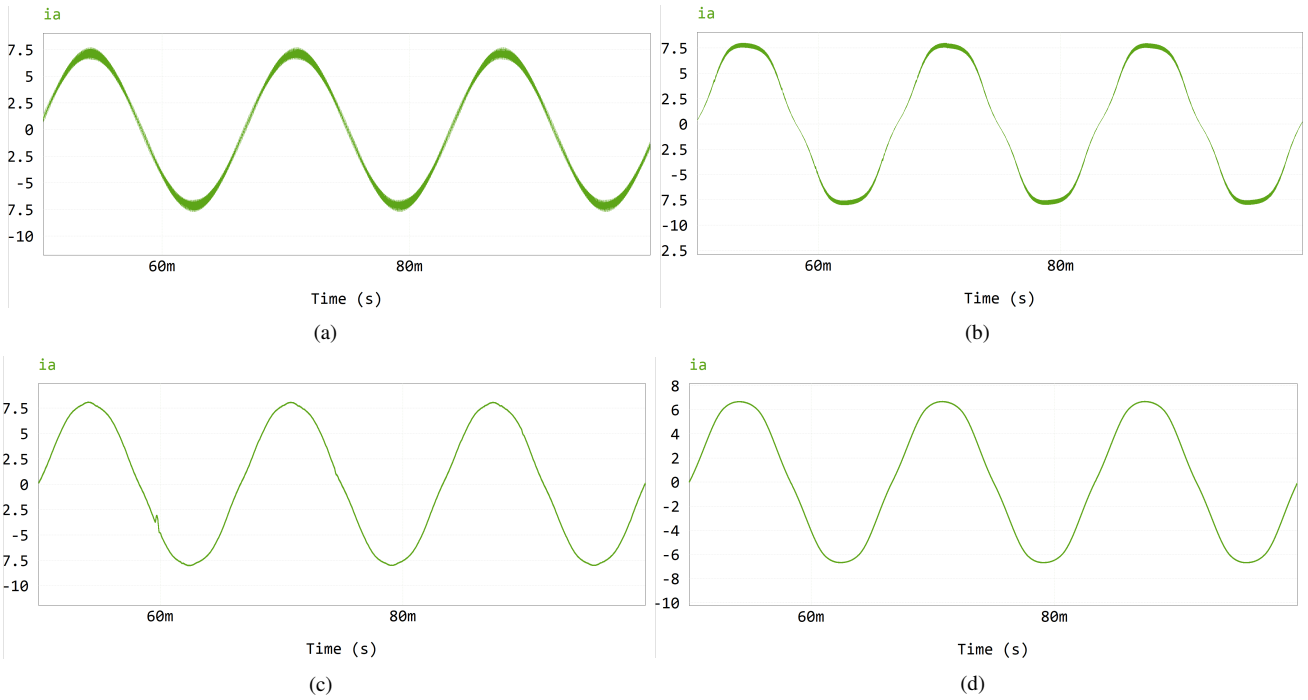

FIGURE 6. Input current comparison: (a) Two-level three-phase boost CCM rectifier; (b) Three-phase boost DCM rectifier; (c) Three-level three-phase interleaved boost DCM rectifier; (d) Dual input interleaved DCM three-phase rectifier.

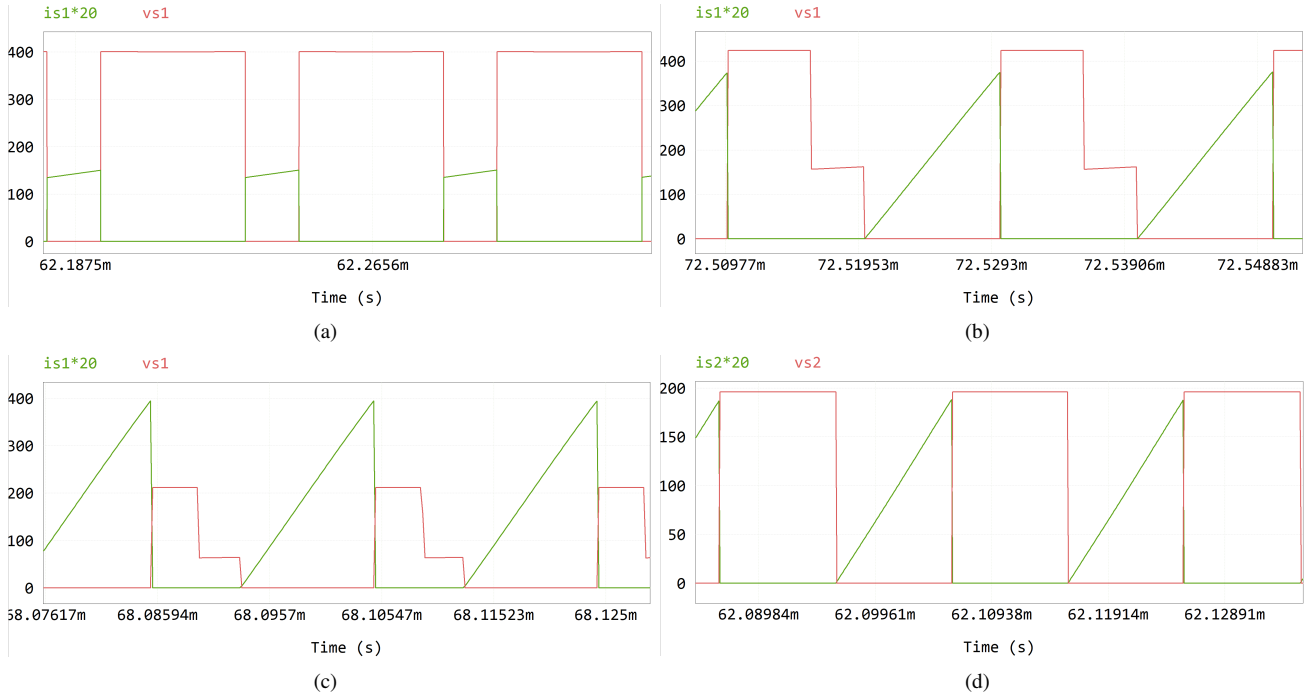

FIGURE 7. Comparison of the waveforms of the voltage across the switch, v_s, and the current through the switch, i_s (a) Two-level three-phase boost CCM rectifier; (b) Three-phase boost DCM rectifier; (c) Three-level three-phase interleaved boost DCM rectifier; (d) Dual input interleaved DCM three-phase rectifier.

the substantially lower inductance value compared to the CCM topology, and the reduced current stresses compared to the structures operating in DCM. Moreover, in terms of total volume, the proposed rectifier continues to exhibit the smallest value, despite utilizing six input inductors, compared to only three in the other topologies.

Lastly, Table V presents a cost analysis, comparing all rectifiers based on component costs. The main source of

CC BY

TABLE IV. Selected Cores for the Input Inductors

Rectifier	Selected Core	Core volume (cm^3)	Total volume (cm^3)
Two-level three-phase boost CCM rectifier [23]	E-65/13	36.4	109.2
Three-phase boost DCM rectifier [13], [14]	E-42/15	17.6	52.8
Three-level three-phase interleaved boost DCM rectifier [17]	E-42/15	17.6	52.8
Dual input interleaved three-phase rectifier	E-30/14	8	48

information regarding the price of the components was the DigiKey Electronics website. For this evaluation, the configuration considered for the dual input interleaved DCM three-phase rectifier is configuration 02, presented in Table I. Additionally, for the inductors, only the core costs were considered to simplify the quotation process. This analysis indicates that the most expensive topology is the three-level three-phase interleaved Boost DCM rectifier [17], followed by the dual input interleaved three-phase rectifier.

IV. EXPERIMENTAL RESULTS

To validate the rectifier's operation, experimental tests were conducted with a programmable three-phase power supply, model ITECH IT7625, 300 V AC, 12 A RMS, and a maximum power of 4.5 kVA. In order to emulate a DC bus controlled by an inverter, to which the rectifier would be connected in a real-life application, a programmable DC power supply, model FCC 350-100i, was used to establish a fixed voltage of 400 V on the rectifier output bus. A power analyzer, model Fluke Norma 4000, was used to measure the converter's output power and efficiency. The rectifier's specifications utilized for the tests can be found in Table VI, images of the constructed prototype are shown in Fig. 8 (top view) and Fig. 9 (side view), and the experimental setup is presented in Fig. 10.

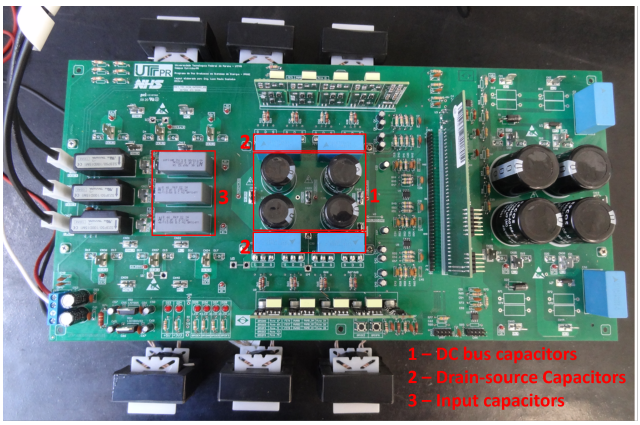

FIGURE 8. Rectifier prototype board - top view.

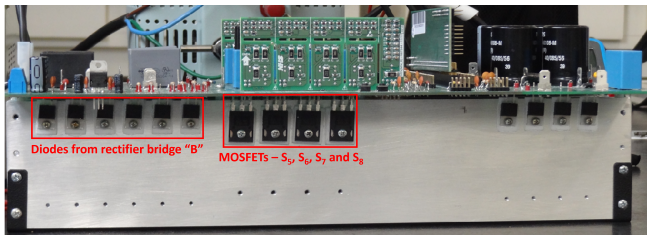

FIGURE 9. Rectifier prototype board - side view.

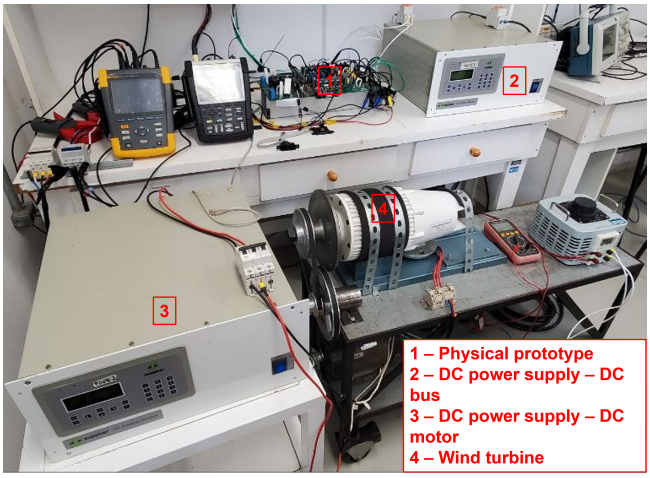

FIGURE 10. Experimental setup.

The rectifier's efficiency curve, shown in Fig. 11, was obtained by controlling the converter's output power as the duty cycle was adjusted accordingly. Measures were acquired for six different values of output power: 200 W, 400 W, 600 W, 800 W, 900 W and 1 kW. The waveforms of the input currents and the input capacitor voltage of phase A (v_{C_a}), for an output power of 1 kW, can be seen in Fig. 12. The waveforms of the currents flowing through inductors L_{A_a} and L_{B_a} can be found in Fig. 13. The THD of the input current i_a, and the rectifier's power factor, for an output power of 1 kW, are presented in Fig. 14 and Fig. 15, respectively. As can be seen in Fig. 13, the rectifier operates in DCM, and Fig. 12 demonstrates its operation with sinusoidal input currents, containing a low ripple. Fig. 15 indicates a high power factor of 0.997, and Fig. 14 shows

TABLE V. Component Price Analysis

Topology	Component	Part Number	Price ($) (Unit)	Total Price ($)	Total Cost
Two-level three-phase boost CCM rectifier	1 x CAP ALUM 240UF 20% 450V	EKHJ451VSN241MR35M	$ 8.40	$ 8.40	$ 24.84
	6 x IGBT 600V 7.5A DPAK	STGD3HF60HDT4	$ 1.37	$ 8.22	
	3 x Inductor core NEE-65/33/13-3600	THORNTON - 215465	$ 2.74	$ 8.22	
Three-phase boost DCM rectifier	1 x CAP ALUM 240UF 20% 450V	EKHJ451VSN241MR35M	$ 8.40	$ 8.40	$ 30.46
	1 x MOSFETs Power TRS, 600V/16A	RJK6014DPP-E0#T2	$ 5.54	$ 5.54	
	7 x DIODE GEN PURP 200V 6A	SF64G	$ 0.80	$ 5.60	
	3 x CAP PP 3.3UF 10% 200V RADIAL	399-R71VN433050H6K-ND	$ 2.70	$ 8.10	
	3 x Inductor core NEE-42/21 /15-4000	THORNTON - 214515	$ 0.94	$ 2.82	
Three-level three-phase interleaved boost DCM rectifier	2 x CAP ALUM 470UF 20% 250V SNAP TH	B43505A2477M000	$ 6.31	$ 12.62	$ 50.05
	2 x MOSFET N-CH 300V 15A TO220FL	H5N3007FL-M0-E#T2	$ 3.61	$ 7.22	
	8 x DIODE GEN PURP 300V 8A DPAK	SDURD830	$ 0.63	$ 5.04	
	3 x CAP PP 5.1UF 5% 200V RADIAL	MKP385551040JPI2T0	$ 7.45	$ 22.35	
	3 x Inductor core NEE-42/21 /15-4000	THORNTON - 214515	$ 0.94	$ 2.82	
Dual input interleaved three-phase rectifier	2 x CAP ALUM 470UF 20% 250V SNAP TH	B43505A2477M000	$ 6.31	$ 12.62	$ 38.08
	4 x MOSFET N-CH 300V 7A D2PAK	FQB7N30TM	$ 0.78	$ 3.12	
	3 x CAP PP 1.8UF 5% 250V RADIAL	399-R75PR4180AA30J-ND	$ 2.64	$ 7.92	
	16 x DIODE GEN PURP 300V 4A DO201AD	SF45G	$ 0.71	$ 11.36	
	6 x Inductor core NEE-30/15/14-4000	THORNTON - 215902	$ 0.51	$ 3.06	

TABLE VI. Experimental Tests Parameters

Parameter	Value
Maximum output power	1 kW
DC bus voltage	400 V
Input line voltage (RMS)	114 V
Switching frequency	51.4 kHz
Input inductance	80.7 μH
Input capacitance	2 μF
Output capacitance	2x470 μF

a low THD of i_a, measured at 2.08%. Furthermore, the converter's efficiency presented satisfactory results, being above 95% for the maximum output power applied, as depicted in Fig. 11.

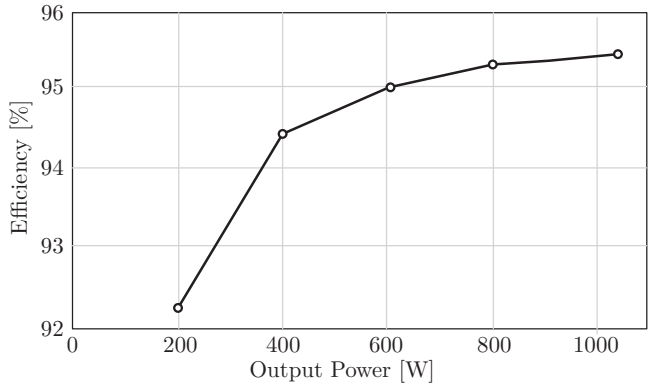

FIGURE 11. Rectifier's efficiency curve.

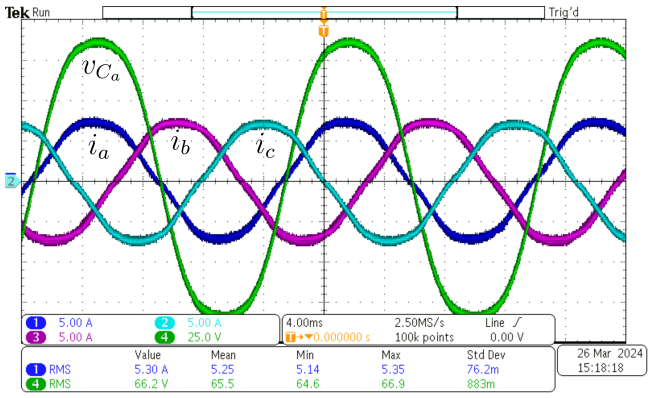

FIGURE 12. Input currents (i_a, i_b and i_c) and input capacitor voltage of phase A (v_{C_a}).

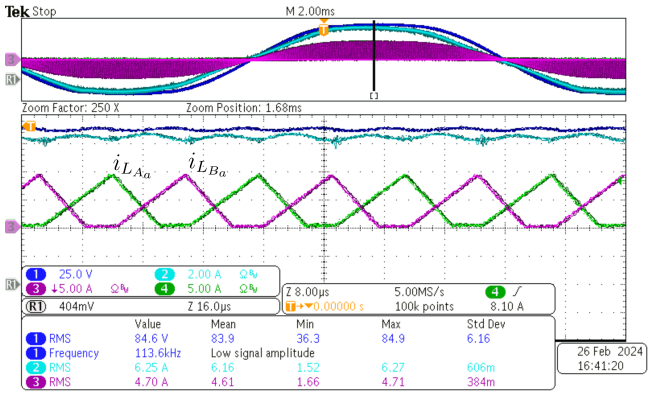

FIGURE 13. Currents in inductors L_{A_a} and L_{B_a}.

To assess the rectifier's performance when connected to a small wind turbine, experiments were executed using a wind turbine whose technical specifications are detailed in Table VII. To perform the experiments, the turbine was

CC BY

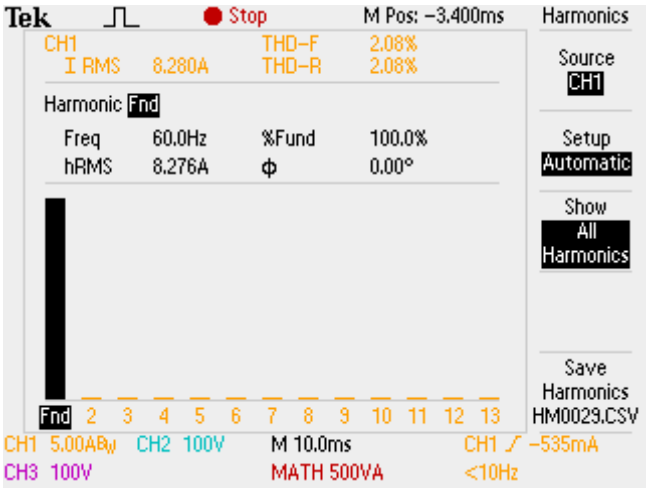

FIGURE 14. Experimental THD of input current i_a.

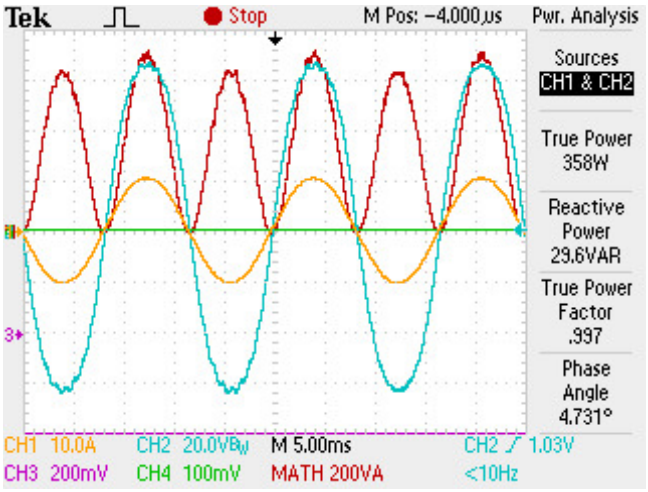

FIGURE 15. Experimental power factor.

connected to a DC motor powered by a DC power source, model FCCT 400-10-I. In this scenario, the MPP of the system is determined by the maximum power delivered by the DC source. Fig. 16 illustrates the waveforms of the input currents and the input capacitor voltage of phase A (v_{C_a}) when operating with the wind turbine, while Fig. 17 presents these waveforms for transient response condition. The experimental results presented in Fig. 16 demonstrate that the rectifier still operates with sinusoidal input currents, with a high power factor, and the results presented in Fig. 17, show that the input current waveform follows the input voltage waveform from the moment the system is turned on.

TABLE VII. Wind Turbine Parameters

Parameter	Value
Maximum output power	2 kW
Turbine radius	1.6 m
Maximum wind speed	10 m/s
Maximum line voltage RMS	96 V

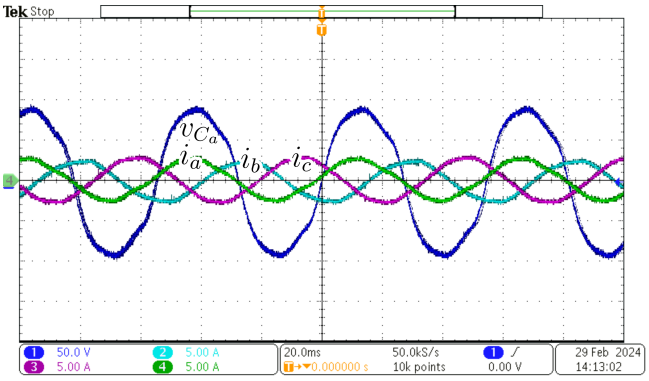

FIGURE 16. Input currents (i_a, i_b and i_c) and input capacitor voltage of phase A (v_{C_a}) when operating with the wind turbine.

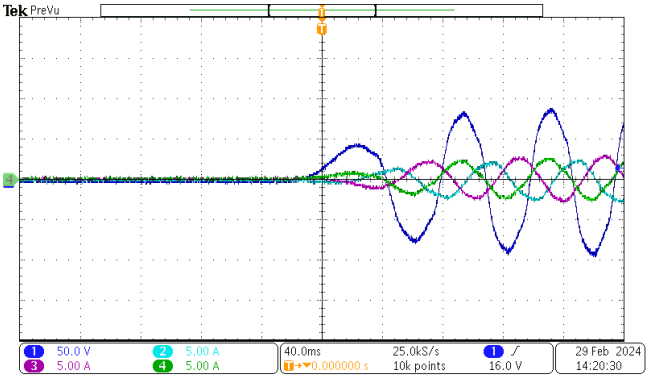

FIGURE 17. Rectifier's transient response when operating with the wind turbine.

To further analyze the converter's operation with the small wind generator, experimental tests were carried out utilizing the MPPT strategy presented in Section II.C. The controller utilized was the digital signal controller (DSC) 56F84789 from NXP Semiconductors. During the experiments, an energy analyzer, model Fluke 434, was used to record data of the converter's input power, input RMS line voltages, and input RMS phase currents. Fig. 18 presents the wind turbine power over time, and Fig. 19 illustrates the wind turbine power in function of the RMS line voltage v_{ac}, which is proportional to the wind turbine rotation speed. As it is possible to observe in both Figures, the MPPT algorithm successfully tracked the point of maximum power, and the converter operates consistently around the obtained value (close to 390 W).

V. CONCLUSION

This article proposes a rectifier topology for operation in the rectifier stage of small wind power systems, considering power levels below 15 kW. The converter, which operates in discontinuous conduction mode, can handle variable input voltages (as occurs in variable speed wind turbines), and the dual-input configuration allows for higher power demand ap-

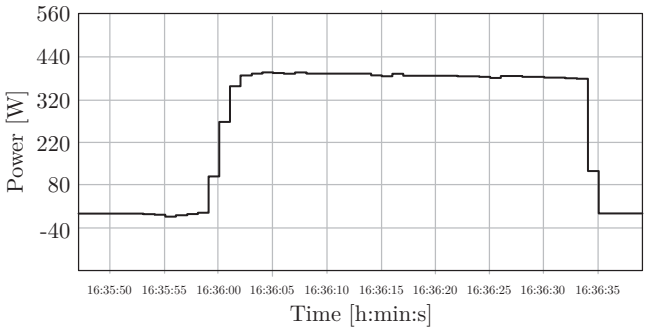

FIGURE 18. Windturbine power vs Time.

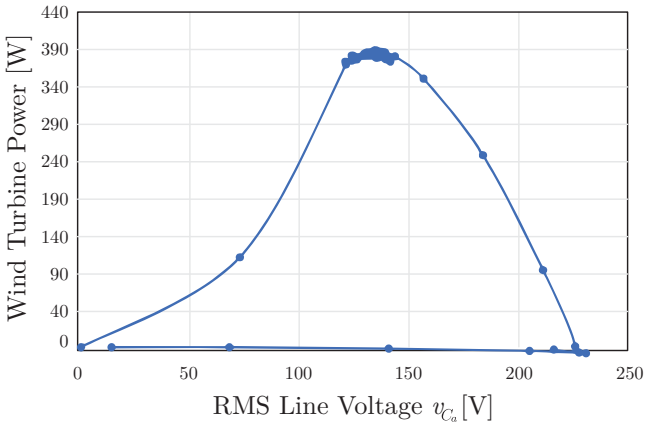

FIGURE 19. Windturbine power vs RMS line voltage v_{ac}.

plications compared to single-input structures, as the current stresses are shared between the two diode bridges.

The simulation study demonstrated that the current stresses throughout the entire structure of the proposed three-phase rectifier are significantly reduced compared to the two other topologies operating in DCM. In fact, they are close to those in the CCM topology, despite utilizing input inductances approximately 15 times smaller. Moreover, the inductor core designed for the proposed rectifier had the smallest volume — nearly five times smaller than that of the CCM topology and about half the size of the cores used in the other DCM topologies. Thus, even though the proposed converter uses six input inductors, the reduced current stress, combined with lower inductance values, offers a reduction in both cost and volume of these components compared to the DCM and CCM structures that use three input inductors.

Experiments were performed in order to validate the rectifier's operation characteristics, employing a three-phase power supply, a wind turbine, and a wind turbine in conjunction with an MPPT method. The experimental results from all three scenarios demonstrate that the converter operated with sinusoidal input currents, exhibited low current ripple, and achieved a high power factor. Additionally, the rectifier's efficiency at the maximum applied output power (1 kW) exceeded 95%.

Therefore, the proposed rectifier is suitable for applications in small wind turbines, presenting a topology with high gain and considerably reduced current stresses.

ACKNOWLEDGMENT

The authors gratefully acknowledge the efforts of Murilo P. de Oliveira and Michell L. Stiz during the experimental results acquisition. They would also like to express their sincere gratitude to the Brazilian company NHS Sistemas de Energia for the provided financial support.

AUTHOR'S CONTRIBUTIONS

G. M. TODYS: Conceptualization, Data Curation, Formal Analysis, Investigation, Methodology, Project Administration, Software, Validation, Visualization, Writing – Original Draft, Writing – Review & Editing. **L. P. CUSTÓDIO**: Conceptualization, Formal Analysis, Investigation. **A. A. BADIN**: Funding Acquisition, Project Administration, Resources, Supervision, Writing – Review & Editing. **A. A. ASSEF**: Investigation, Methodology, Project Administration, Resources, Software, Supervision, Writing – Review & Editing. **R. GULES**: Conceptualization, Data Curation, Formal Analysis, Investigation, Methodology, Project Administration, Supervision, Validation, Writing – Original Draft, Writing – Review & Editing. **D. G. BANDEIRA JR.**: Software, Supervision, Validation, Writing – Review & Editing. **E. F. R. ROMANELI**: Funding Acquisition, Project Administration, Resources, Supervision. **D. F. CORTEZ**: Conceptualization, Data Curation, Formal Analysis, Investigation, Methodology, Project Administration, Supervision, Validation, Writing – Original Draft, Writing – Review & Editing.

PLAGIARISM POLICY

This article was submitted to the similarity system provided by Crossref and powered by iThenticate – Similarity Check.

REFERENCES

[1] F. Blaabjerg, Y. Yang, K. A. Kim, J. Rodriguez, "Power Electronics Technology for Large-Scale Renewable Energy Generation", *Proceedings of the IEEE*, vol. 111, no. 4, pp. 335–355, 2023, doi:10.1109/JPROC.2023.3253165.

[2] M. Z. Malik, M. H. Baloch, B. Ali, S. H. Khahro, A. M. Soomro, G. Abbas, S. Zhang, "Power Supply to Local Communities Through Wind Energy Integration: An Opportunity Through China-Pakistan Economic Corridor (CPEC)", *IEEE Access*, vol. 9, pp. 66751–66768, 2021, doi:10.1109/ACCESS.2021.3076181.

[3] P. Roy, J. He, T. Zhao, Y. V. Singh, "Recent Advances of Wind-Solar Hybrid Renewable Energy Systems for Power Generation: A Review", *IEEE Open Journal of the Industrial Electronics Society*, vol. 3, pp. 81–104, 2022, doi:10.1109/OJIES.2022.3144093.

[4] Z. Wang, Y. Jia, C. Cai, Y. Chen, N. Li, M. Yang, Q. Li, "Study on the Optimal Configuration of a Wind-Solar-Battery-Fuel Cell System Based on a Regional Power Supply", *IEEE Access*, vol. 9, pp. 47056–47068, 2021, doi:10.1109/ACCESS.2021.3064888.

[5] C. Breyer, S. Khalili, D. Bogdanov, M. Ram, A. S. Oyewo, A. Aghahosseini, A. Gulagi, A. A. Solomon, D. Keiner, G. Lopez, P. A. Østergaard, H. Lund, B. V. Mathiesen, M. Z. Jacobson, M. Victoria, S. Teske, T. Pregger, V. Fthenakis, M. Raugei, H. Holttinen, U. Bardi, A. Hoekstra, B. K. Sovacool, "On the History and Future of 100%

Renewable Energy Systems Research", *IEEE Access*, vol. 10, pp. 78176–78218, 2022, doi:10.1109/ACCESS.2022.3193402.

[6] F. Stadtmann, A. Rasheed, T. Kvamsdal, K. A. Johannessen, O. San, K. Kölle, J. O. Tande, I. Barstad, A. Benhamou, T. Brathaug, T. Christiansen, A.-L. Firle, A. Fjeldly, L. Frøyd, A. Gleim, A. Høiberget, C. Meissner, G. Nygård, J. Olsen, H. Paulshus, T. Rasmussen, E. Rishoff, F. Scibilia, J. O. Skogås, "Digital Twins in Wind Energy: Emerging Technologies and Industry-Informed Future Directions", *IEEE Access*, vol. 11, pp. 110762–110795, 2023, doi:10.1109/ACCESS.2023.3321320.

[7] F. Blaabjerg, K. Ma, "Future on Power Electronics for Wind Turbine Systems", *IEEE Journal of Emerging and Selected Topics in Power Electronics*, vol. 1, no. 3, pp. 139–152, 2013, doi:10.1109/JESTPE.2013.2275978.

[8] F. Blaabjerg, K. Ma, "Wind Energy Systems", *Proceedings of the IEEE*, vol. 105, no. 11, pp. 2116–2131, 2017, doi:10.1109/JPROC.2017.2695485.

[9] M. M. Xavier, *et al.*, *Retificador SEPIC trifásico isolado operando em DCM para aplicação em aerogeradores de pequeno porte*, Master's thesis, Universidade Tecnológica Federal do Paraná, 2022.

[10] P. J. S. Costa, T. B. Lazzarin, F. A. B. Batista, C. H. I. Font, "Conexão de Aerogeradores de Pequeno Porte em Microrredes de Corrente Contínua Utilizando um Retificador Trifásico Modular Sepic", *Eletrônica de Potência*, vol. 21, no. 3, p. 212–223, Sep. 2016, doi:10.18618/REP.2016.3.2606, URL: https://journal.sobraep.org.br/index.php/rep/article/view/285.

[11] R. H. Eckstein, T. B. Lazzarin, I. Barbi, "Proposed power and control system for small scale wind turbines connected to the grid", *in 3rd Renewable Power Generation Conference (RPG 2014)*, pp. 1–6, 2014, doi:10.1049/cp.2014.0836.

[12] K. Buchert, F. W. Fuchs, "Comparison of three phase rectifier topologies in small wind turbines", *in 2014 16th European Conference on Power Electronics and Applications*, pp. 1–10, 2014, doi:10.1109/EPE.2014.6910894.

[13] A. Prasad, P. Ziogas, S. Manias, "An active power factor correction technique for three-phase diode rectifiers", *IEEE Transactions on Power Electronics*, vol. 6, no. 1, pp. 83–92, 1991, doi:10.1109/63.65006.

[14] D. Vilathgamuwa, S. Jayasinghe, "Rectifier systems for variable speed wind generation - a review", *in 2012 IEEE International Symposium on Industrial Electronics*, pp. 1058–1065, 2012, doi:10.1109/ISIE.2012.6237235.

[15] L. Jianlin, H. Shuju, X. Honghua, "A kind of direct-driven WECS using single-switch three-phase Boost rectifier", *in 2008 IEEE International Conference on Industrial Technology*, pp. 1–6, 2008, doi:10.1109/ICIT.2008.4608557.

[16] A. Nabae, H. Nakano, S. Arai, "Novel sinusoidal converters with high power factor", *in Proceedings of 1994 IEEE Industry Applications Society Annual Meeting*, vol. 2, pp. 775–780 vol.2, 1994, doi:10.1109/IAS.1994.377506.

[17] M. H. Granza, R. Gules, C. H. Illa Font, "Hybrid and Three-Level Three-Phase Rectifiers Using Interleaved DCM Boost Converters", *IEEE Access*, vol. 7, pp. 160168–160176, 2019, doi:10.1109/ACCESS.2019.2951123.

[18] M. H. Granza, *et al.*, *Conversores CA-CC multinívels do tipo boost com elevado fator de potência e operação em condução descontínua: estudo de topologias monofásicas, trifásicas, não isolados e isoladas*, Ph.D. thesis, Universidade Tecnológica Federal do Paraná, 2020.

[19] G. M. Todys, A. A. Badin, A. A. Assef, D. F. Cortez, D. G. Bandeira, E. F. R. Romaneli, L. P. Custódio, R. Gules, "Interleaved Three-Phase Rectifier Dual Input Single Stage In Discontinuous Conduction Mode With Maximum Power Tracking Method For Application In Small Wind Generators", *in 2023 IEEE 8th Southern Power Electronics Conference and 17th Brazilian Power Electronics Conference (SPEC/COBEP)*, pp. 1–7, 2023, doi:10.1109/SPEC56436.2023.10407550.

[20] L. d. O. Stamm, *et al.*, *Retificadores trifásicos três níveis em modo de condução descontínua para geração eólica de baixa potência*, Master's thesis, Universidade Tecnológica Federal do Paraná, 2022.

[21] N. Swaminathan, N. Lakshminarasamma, Y. Cao, "A Fixed Zone Perturb and Observe MPPT Technique for a Standalone Distributed PV System", *IEEE Journal of Emerging and Selected Topics in Power Electronics*, vol. 10, no. 1, pp. 361–374, 2022, doi:10.1109/JESTPE.2021.3065916.

[22] M. H. Ibrahim, S. P. Ang, M. N. Dani, M. I. Rahman, R. Petra, S. M. Sulthan, "Optimizing Step-Size of Perturb Observe and Incremental Conductance MPPT Techniques Using PSO for Grid-Tied PV System", *IEEE Access*, vol. 11, pp. 13079–13090, 2023, doi:10.1109/ACCESS.2023.3242979.

[23] Z. Chen, J. M. Guerrero, F. Blaabjerg, "A Review of the State of the Art of Power Electronics for Wind Turbines", *IEEE Transactions on Power Electronics*, vol. 24, no. 8, pp. 1859–1875, 2009, doi:10.1109/TPEL.2009.2017082.

BIOGRAPHIES

Guilherme M. Todys was born in Curitiba, Brazil, in 1995, and received the B. S. degree in electrical engineering from the Federal Technological University of Paraná – UTFPR, Curitiba, Brazil, in 2021. He is currently working towards the Master's degree in electrical engineering at the Postgraduate Program in Energy Systems - PPGSE, at the Federal Technological University of Paraná, being part of the research team at the Electronic Energy Processing Laboratory (LPEE) at UTFPR. His areas of interest include renewable energy processing, high power factor rectifiers, and power factor correction techniques.

Luís P. Custódio received the B.S. and M.S. degrees in electrical engineering from the Federal Technological University of Paraná – UTFPR, Curitiba, Brazil, in 2017 and 2021 respectively. His areas of interest include power electronics, power systems, renewable energy, and Wireless power transfer.

Alceu A. Badin (Member, IEEE) was born in Maravilha, Santa Catarina, Brazil, in 1979. He received the B.S., M.S., and Ph.D. degrees in electrical engineering from the Federal University of Santa Catarina, Florianopolis, Brazil, in 2002, 2004, and 2009, respectively. Since 2010, he has been a Professor at the Federal Technological University of Paraná – UTFPR, Curitiba, Brazil. His current research interests include high-frequency power converter topologies, power factor correction techniques, and power supplies. Prof. Badin is a Member of the Brazilian Power Electronic Society and IEEE Power Electronics Society.

Amauri A. Assef received the B.S. degree in electrical engineering, and the M.Sc. and Ph.D. degrees in science and biomedical engineering from the Federal Technological University of Paraná – UTFPR, Curitiba, Brazil, in 1999, 2006, and 2013, respectively. Since 2009, he has been a Professor of Electrical Engineering at the Federal Technological University of Paraná – UTFPR, Curitiba. His research interests include ultrasound and electronic instrumentation.

Daniel Flores Cortez born in Pelotas, Rio Grande do Sul, Brazil, in 1985. He received the B.S. degree from the Catholic University of Pelotas - UCPel, Pelotas (RS), Brazil, in 2009, and the M.S. and Ph.D. degrees in electrical engineering from the Federal University of Santa Catarina, Florianopolis, Brazil, in 2012 and 2015, respectively. Since 2015, he has been a Professor of Electrical Engineering at the Federal Technological University of Paraná – UTFPR, Curitiba, Brazil. His current research interests include dc/dc bidirectional converters, switched-capacitors, and power factor correction techniques.

Delvanei Gomes Bandeira Jr. was born in Pelotas, RS, Brazil, in 1986. He received the B.S. degree in electrical engineering from the Catholic University of Pelotas, Pelotas RS, Brazil, in 2011, and the M.Sc. and Ph.D. degrees in electrical engineering from the Federal University of Santa Catarina, Florianopolis, SC, Brazil, in 2014 and 2019 respectively. Since 2019, he has been a Professor of Electrical Engineering at the

Federal Technological University of Paraná – UTFPR, Curitiba. His research interests include soft switching, switched capacitors, and high-voltage power supplies.

Eduardo F. R. Romaneli was born in Londrina, Paraná, Brazil, in 1970. He received the B.S., M.S., and Ph.D. degrees in Electrical Engineering from the Federal University of Santa Catarina, Florianópolis, Brazil, in 1993, 1998, and 2001, respectively. Since 2003, he has been a Full-Time Professor of Electrical Engineering at the Federal Technological University of Paraná – UTFPR, Curitiba, Brazil. His research has spanned several disciplines, emphasizing power electronics. His current research interests are focused on uninterruptible power systems, power-factor correction, and renewable energy processing.

Roger Gules (Member, IEEE) was born in Bento Gonçalves, Brazil, in 1971. He received the B.S. degree from the Federal University of Santa Maria (UFSM), Santa Maria, Brazil, in 1995, and the M.S. and Ph.D. degrees from the Federal University of Santa Catarina (UFSC), Florianópolis, Brazil in 1998 and 2001, respectively, all in electrical engineering. From 2001 to 2005, he was a Professor at the Universidade do Vale do Rio dos Sinos, São Leopoldo, Brazil. Since 2006, he has been a Professor of Electrical Engineering at the Federal Technological University of Paraná – UTFPR, Curitiba, Brazil. His research interests include high-frequency power conversion, renewable energy applications, and high-power factor rectifiers.

CC BY